THE UNIVERSITY OF CHICAGO

PLACING LIMITS ON EXPERIMENTAL SIGNATURES OF DARK MATTER MODEL PREDICTIONS

A DISSERTATION SUBMITTED TO
THE FACULTY OF THE DIVISION OF THE PHYSICS
IN CANDIDACY FOR THE DEGREE OF
DOCTOR OF PHILOSOPHY

DEPARTMENT OF PHYSICS

BY
ARJUN SHARMA

CHICAGO, ILLINOIS
AUGUST 2018

To My Friends And Family

TABLE OF CONTENTS

LIST OF FIGURES

ACKNOWLEDGMENTS

I would like to thank my family for supporting me during the turbulence of the last few years as I have tried to balance work and my studies.

I want to thank Chris Kelso for being a colleague as well as mentor in the process of writing my dissertation.

I want to thank Pf Yau Wah, Dr David Reid, Young-Kee Kim for being on my committee and helping me finish up.

Many thanks to my brothers/friends Sagar Sharma, Amod Timilsina and Balindra Tripathi for friendly encouragement and tough talk when I needed it.

ABSTRACT

In this work, we consider two different models of dark matter and set limits on results of experiments. One is a dynamical dark matter scenario where we put limits on parameters observable by experiments DAMA and XMASS through nuclear recoil of detector atoms (direct detection). The second is a case of dark matter annihilation into positrons and electrons and the signal this would produce on measured values of positron flux and ratio of electron to positron (indirect detection). The values of these quantities as measured by FERMI and PAMELA experiments are observed and an explanation using a dark matter annihilation is presented vs astrophysical sources of particles.

We explore a dynamical dark matter scenario with an ensemble of dark matter particles that starts at m_0 and spans a comb of particles separated by $j^\delta \Delta m$. We verify the model by using $\Delta m = \infty$ and comparing the predictions to a non dynamical model for the same mass m_0. We then observe the wider set of possibilities available with the dynamical dark matter model compared with the single mass case vis a vis constraints set by NaI and Xe detectors published by the DAMA and XMASS collaborations and check for validity of model against these measurements.

The Fermi experiment has measured the cosmic ray electron+positron spectrum and positron fraction $[\Phi_{e^+}/(\Phi_{e^+ + e^-})]$, and PAMELA has measured the positron fraction with better precision. While the majority of cosmic ray electrons and positrons are of astrophysical origin, there may also be a contribution from dark matter annihilation in the galactic halo. The upcoming results of the AMS experiment will show measurements of these quantities with far greater precision. One dark matter annihilation scenario is where two dark matter particles annihilate directly to e^+ and e^- final states. In this article, we calculate the signature "bumps" in these measurements assuming a given density profile (NFW profile). If

the dark matter annihilates to electrons and positrons with a cross section $\sigma v \sim 10^{-26}$ cm^3/s or greater, this feature may be discernible by AMS. However, we demonstrate that such a prominent spectral feature is already ruled out by the relative smoothness of the positron + electron cosmic ray spectrum as measured by Fermi. Hence we conclude that such a feature is undetectable unless the mass is less than $\sim$40 GeV.

CHAPTER 1

INTRODUCTION

1.1 Dark Matter Background

There is a significant amount of evidence supporting the existence of matter that is detectable through its gravitational effects but is not composed of standard baryonic particles. This dark matter does not interact with light at a significant level but constitutes the preponderant fraction of the gravitational mass in the cosmos. A relatable analogy: you look at a child sitting on a trampoline but notice that the depression on the fabric is much deeper than you would expect. You photograph and take x-ray pictures of the child and it is a completely normal child, yet the depression on the trampoline is anomalously large. Hence you deduce that the child has an invisible dark matter halo around him. The exciting task of explaining the nature of this dark component is underway and this work is a contribution to that effort. Detection using direct and indirect experiments as well as colliders are in operation and limits predicted by theoretical models are being tested.

Evidence for dark matter comes from astrophysical and cosmological observations. Measurements of the motion of stars near the Galactic plane were first imputed to the gravitational influence of unseen mass [1]. In 1933, Fritz Zwicky studied the dynamics of the galaxies of the Coma cluster, saw that the the velocities of galaxies were larger than expected and postulated unseen mass to explain his observations and coined the term 'dark matter' [2]. Flattening of galactic rotation curves at radii larger than the visible edges, as well as strong and weak gravitational lensing in galaxies and clusters are well studied astrophysical phenomena that build the case for the existence of dark matter [7, 8]. The bullet cluster shows a clear spatial separation of the gravitational center of mass (measured using gravitational lensing) and the location of the visible

baryonic matter (measured by X-ray imaging of hot gas) [4] -in our analogy, the child has jumped off to the side but the trampoline is still depressed in the middle .

Studies of anisotropies in the cosmic microwave background (CMB) allow for a constraint on the density of dark-matter density in units of the critical density of the Universe at $\Omega_{dm} = 0.222 \pm 0.026$ [9]. Measurements of the abundances of light elements produced during the big-bang nucleosynthesis put the density of baryonic matter to be $\Omega_b = 0.0449 \pm 0.0028$. We can see that non-baryonic dark matter comprises the majority ($\approx 80\%$) of the matter in the Universe, and hence about a quarter of the total amount of matter-energy.

Despite evidence for the abundant existence of dark matter in the universe, the nature of dark matter is still unknown. It is possible that dark matter interacts only through the relatively weak force of gravity and this could be the reason we have only seen gravitational effects so far. However particle physics theories that allow for dark matter to interact with baryonic particles with other forces exist and also explain current issues in the standard model. One of these is weakly interacting massive particles (WIMP).

1.2 Weakly Interacting Massive Particles WIMP's

We consider the weakly interacting massive particles as relics of thermal freeze out and relate the density to cosmological evolution. Let's take a stable dark matter particle, X that interacts with Standard Model particles Y through some process $X\overline{X} \leftrightarrow Y\overline{Y}$. In the dense, high temperature early universe, where the temperature was much greater than m_X, the mass of the particle X, the creation/annihilation processes of $X\overline{X}$ (left and right arrow direction) were equally efficient. Therefore, abundant amounts of X was present along with the other particles of the Standard Model in thermal equilibrium with the photon bath. As the universe expanded and

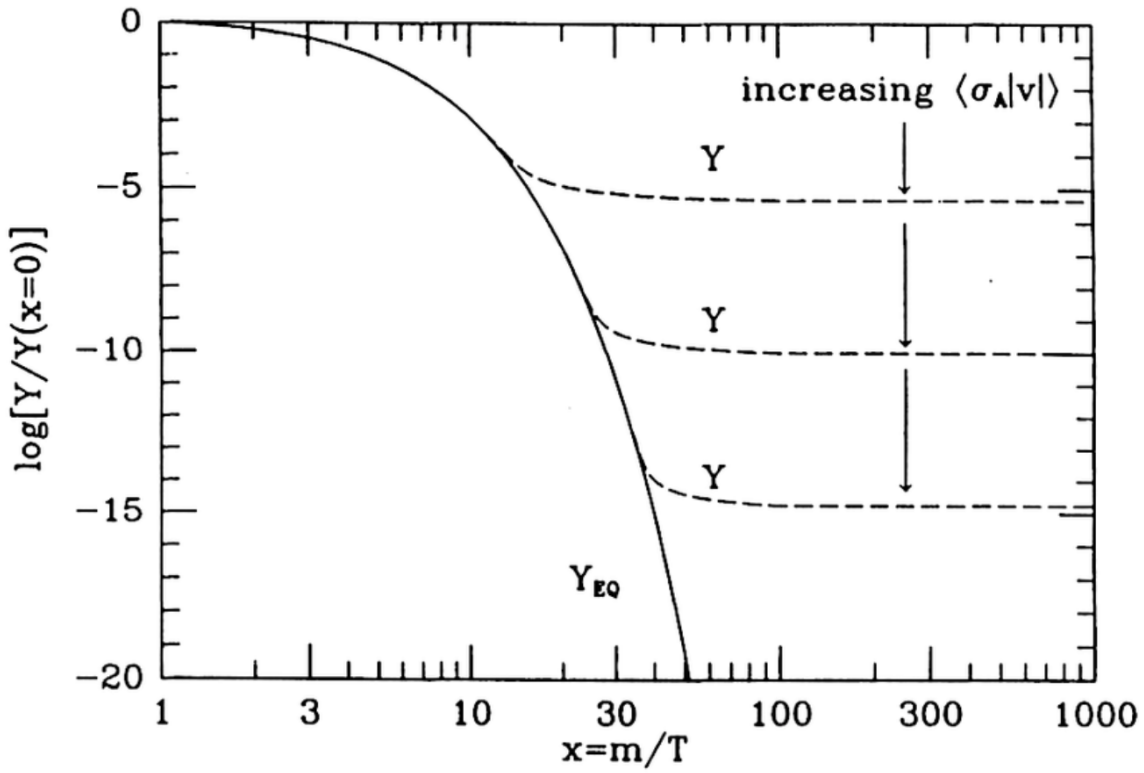

Figure 1.1: Schematic: Evolution of comoving number density of a stable particle through process of thermal freeze-out. Fig source: [5]

.

the density and hence temperature fell below m_X, the annihilation rate remained steady, however the process of $X\overline{X}$ creation became exponentially suppressed because of the Boltzmann factor. For these particles in thermal equilibrium at temperatures T $\ll m_X$, the number density is given by:

$$n_X = g_X(\frac{m_X T}{2\pi})^{3/2} e^{-m_X/T} \tag{1.1}$$

where g_X is the number of internal degrees of freedom of X. As the temperature, T decreases, the exponential factor quickly supresses this number density in an expanding (cooling) universe.

This exponential supression of number density is counteracted by the Hubble

expansion because the effective reduction in density limits the collision rate. As the density decreases due to expansion, the annihilation rate becomes sufficiently small that a certain density of these particles can survive and remain until the present. The Boltzmann equation describing the density of particles X is given by:

$$\frac{dn_X}{dt} + 3Hn_X = - < \sigma_{X\overline{X}} \| v \| > (n^2_{\overline{X},eq} n^2_{X,eq}) \tag{1.2}$$

where H is the Hubble expansion rate of the universe , n_X the number density of WIMP's, and $< \sigma_{X\overline{X}} \| v \| >$ is the thermally averaged annihilation cross section of the $X\overline{X}$. In Fig 1.1, we plot the number density as the temperature decreases (time increases on the positive horizontal axis). As the temperature decreases below the mass of particle X, eventually the Hubble expansion suppresses the annihilations and the number density reaches a steady state. This state reached is an interplay between the annihilation rate and temperature of the universe is known as thermal freeze out. By measuring the relic(comoving) density of a particle we can deduce its annihilation cross section. This relic abundance can be written in terms of the present day WIMP density and the critical density:

$$\Omega_X h^2 \approx 0.1 \left(\frac{3 * 10^{-26} \text{cm}^3/\text{sec}}{< \sigma_{X\overline{X}} \| v \| >} \right) \tag{1.3}$$

where $h = H/(100\text{km/ sec /Mpc}) \approx 0.7$. As we can see, the relic abundance of the WIMP is inversely proportional to its scattering cross section. A larger cross section allows the particle to remain in thermal equilibrium longer with the cooling universe, and hence the corresponding comoving density is lower. An interesting observation is that a cross section on the order of weak-scale interactions gives a WIMP relic abundance that matches the observed dark matter relic abundance. This coincidence, also known as the WIMP miracle is a reason WIMP's are considered as candidates

for dark matter.

1.3 Direct and Indirect Detection

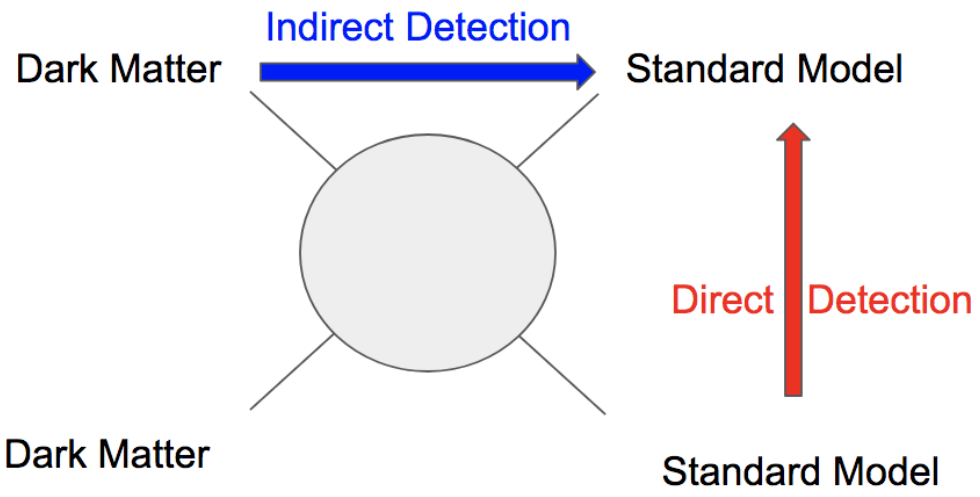

Figure 1.2: Two Dark Matter Detection Schemes Explored in this Work.

While gravitational effects have been observed, the particle nature of dark matter is undiscovered as yet. The experiments being done to uncover this belong to one of three categories: direct detection, indirect detection and collider searches. In Fig. 1.2 we show a schematic of the two methods discussed in this work. The central blob represents the unknown interactions between dark-matter particles and standard model particles. The arrows show the direction of time in the respective experiments. Indirect detection looks at dark matter particles annihilating to produce Standard Model particles. (Colliders, not discussed here, observe standard model particles interacting to produce dark matter particles.) Direct detection is a search for an interaction of dark matter particles with standard model particles

directly. An example is though a nuclear recoil caused by the scattering (with a very small cross section) of a dark matter particle against a standard nucleus. In this work, we look at two modes of experimental verification of dark matter signatures: indirect and direct detection experiments.

In this work, we will consider a scenario in which dark matter particles annihilate to positrons and electrons that might be detectable by indirect detection experiments. Assuming a particular dark matter density profile and dark matter mass, the flux (along with background) will produce a signature feature in the positron+ electron flux and the positron fraction of this flux. Measurements on this flux are made by Pamela, Fermi [19] and AMS experiments [21]. We put constraints on the possible features created by these annihilations on these measurements.

We also examine direct detection experiments in which dark matter particles scatter from detector nuclei (NaI and Xe) as the earth moves in the rest frame of the galactic dark matter halo. These events cause measurable energy depositions in the detectors. The rate of these events will modulate as the earth's motion oscillates across the galactic plane in yearly cycles. We put a limit on features of this modulation as measured by DAMA [14] and XMASS[12] experiments assuming a single mass dark matter particle and a dynamical dark matter ensemble. We also determine the feasibility of future direct detection experiments measuring the difference between this dynamical dark matter model and standard dark matter model.

1.4 Non dynamical vs dynamical Models

One straightforward model for dark matter is to consider a particular dark matter particle X with mass m_X. This particle has to provide the necessary density to explain the mass deficit observed and the scattering cross section has to satisfy the

observed data from numerous detection experiments. Another possibility is a collection of particles of various masses that add up to explain the required signals . In a dynamical dark matter scenario, the dark matter of the universe comprises an ensemble of interacting fields with a variety of masses, mixings, and abundances[11]. In lieu of imposing stability for each field individually, the viability of such a scenario is enforced by requiring that the states with larger masses and Standard-Model decay rates have correspondingly smaller relic abundances, and vice versa. We consider the case of dynamical dark matter model where instead of a single dark matter particle of mass X, we have an ensemble of particles defined by m_0 and Δm.

CHAPTER 2

DYNAMICAL DARK MATTER

2.1 Introduction

Explaining the nature of dark matter has been a standing problem for some time. Direct and indirect detection experiments are being done to probe its nature. Direct detection experiments such as DAMA are one source of data. Dark matter particles interacting with the nuclei of detector elements cause a nuclear recoil, which creates a scintillation that is detected in a photomultiplier tube.

Weakly interacting particles of various masses and interaction cross section, σ, have been considered [10]. This work looks instead at an ensemble of dark matter particles starting at m_0 and spaced by $j^{\delta}\Delta m$ [11]. The densities and couplings of the higher mass particles are written in terms of the base particle and the parameters α, β and δ.

Hence, dark-matter stability is not absolute, but rather depends on the abundances of the various constituents. Such scenarios also allow for a wide range of collider and astrophysical phenomena which extend beyond the possibilities of non dynamical dark matter models.

Extending the work of [10], we consider a dynamical dark matter ensemble as described in [11] and notice the larger range of m_0 and Δm values where a signal consistent with DAMA data [10] is explored. For the set of values (m_0, Δm, σ)that meet this criterion, we also check the DC and annually modulating AC components against the predictions of XMASS using a Xenon detector.

2.2 Experiment and Data

Dark matter particles of mass m_χ scatter off a detector nucleus of atomic mass A with a nuclear recoil energy of Er. Following [11], v is the velocity of the χ in the dark matter halo in the detector rest frame, the quantity v_{min} is the lower limit of kinematic threshold for non-relativistic scattering, where v_e is the velocity of earth with respect to dark matter halo, v_{esc} the galactic escape velocity and v_o the orbital velocity. The energy spectrum for elastic scattering of dark matter with mass m_χ and a nucleus with mass m_N is given by

$$\frac{dR}{dE_{ee}} = \frac{N_T \rho_\chi}{m_\chi} \int_{v_{min}} v f_E(\vec{v}) \frac{d\sigma}{dE_r}(v, E_r) d^3(\vec{v}) \tag{2.1}$$

where ρ_χ is the local dark matter density, N_T is the number of target nuclei per kilogram of the detector, $\frac{d\sigma}{dE_r}(v, E_r)$ is the differential cross section for dark matter-nucleus elastic scattering, $\vec{v}$ is the relative velocity between the dark matter particle and the Earth and $f_E(\vec{v})$ is the normalized (to 1) velocity distribution of the dark matter in the Earth- rest frame. The particles have velocities in a Maxwell Boltzmann distribution, however there is a lower (v_{min}) and upper limit (galactic escape velocity v_{esc}) to the velocities of particles that can interact with detector nuclei at rest on earth.

$$v_{min} = \sqrt{\frac{E_r m_T}{2\mu^2}} \tag{2.2}$$

Here, m_T is the mass of the target nucleus and μ is the reduced mass of the dark matter and target nucleus. We can notice that the lower limit of the velocity, v_{min},

depends on the mass of the dark matter particle (as well as the atomic mass of the detector element). Therefore the contributions to the overall signal of the various mass components, m_χ, will be different. While in a single mass dark matter scenario, we look at individual contributions, an ensemble combines these contributions in the ratios of their abundances. This leads to a wider range of possibilities for an ensemble model.

We will define a few useful parameters in terms of the basic components of the model, i.e. the m_χ, detector elemental mass A, orbital velocity v_0 and the dark matter mass m_χ and $z = v_{esc}/v_o$. The Maxwell-Boltzmann distribution of these dark matter particles in the detector rest frame is truncated on the lower limit by v_{min} and at the upper end by the gravitational escape velocity of the galaxy, v_{esc} to give the expression commonly known as the standard halo model (SHM).

$$f_{SHM}(\vec{u}) = \frac{1}{N_{esc} v_o^3 \pi^{3/2}} \exp(-u^2/v_o^2) \text{ if } u < v_{esc}, \text{ else: } 0 \tag{2.3}$$

where $\vec{u}$ is the velocity of the dark matter particles in the halo rest frame, v_0 is the most likely velocity and N_{esc} is the normalization constant for this truncated Boltzmann distribution.

$$N_{esc} = \text{erf}(z) - \frac{2z}{v_o\sqrt{\pi}} \exp(-z^2) \tag{2.4}$$

The average speed integral, η_{MB}, captures the dependence of the energy spectrum on the velocity distribution and can be calculated for different cases:

$$\eta_l = \frac{\text{erf}(\frac{v_{min}+v_e}{v_o}) + \text{erf}(\frac{-v_{min}+v_e}{v_o}) - \frac{4v_e}{v_o\sqrt{\pi}} \exp(-z^2)}{2v_e N_{esc}} \tag{2.5}$$

$$\eta_h = \frac{\text{erf}(z) + \text{erf}(\frac{-v_{min}+ve}{v_o}) - \frac{2(v_{min}-v_e-v_{esc})}{v_o\sqrt{\pi}} \exp(-z^2)}{2v_e N_{esc}} \tag{2.6}$$

$$\begin{aligned} \eta_{MB} = if\ v_{min} < v_{esc} - ve : \eta_l(v_{min}, v_e) \\ if\ v_{min} < v_e + v_{esc} : \eta_h(v_{min}, v_e) \\ else:\ 0 \end{aligned} \tag{2.7}$$

where v_0 is the orbital velocity, v_e the velocity of the earth, and v_{min} and v_{esc} are the minimum and escape velocities as defined previously.

This summarizes the assumptions made about the dark matter halo constituent particles, the limits on their velocities and their motion as a Maxwell Boltzmann distribution. In this work, we assume a dark matter density of $\rho = .4$ GeVcm^{-3}, $v_0 = 235$ kms^{-1} and $v_{esc} = 550$ kms^{-1}. Similarly, following [10], the assumptions about the nuclear physics of the collisions are summed up in the form factor F, which we write as shown below.

$$F(Er, A) = \frac{3J_1(2m_N E_R R_1)}{\sqrt{2m_N E_R} R_1} \exp(-m_N E_R s^2) \tag{2.8}$$

where E_r is the energy of the collision, A is the atomic mass number of the nucleus, J_1 is the root of the Bessel function of the second kind, and R_1 is given by

$$R_1 = \sqrt{c^2 + \frac{7\pi^2 a^2}{3} - 5s^2} \tag{2.9}$$

where $c \approx 1.23A^{1/3} - 0.06$ fm, $a \approx 0.523$ fm, and $s = 0.9$ fm as determined by fits to

nuclear physics data [17]. When dark-matter particles interact with a target nucleus, nuclear recoils are different for the different isotopes in the detector. Therefore, the expression for the total recoil spectrum is a weighted sum of the contributions of each isotope with its abundance, where A_i and ab_i are the atomic mass and abundance of the i'th isotope. For our study, we have taken $f_{np} = 1$, which is the ratio of dark-matter coupling to neutrons to the dark-matter coupling to protons i.e. the cross section for protons and neutrons is assumed to be equal. The total signal can thus be written as

$$\frac{dR}{dE_r} = m_U N_A \frac{c^2.\rho_{DM}.\sigma_p}{2m_\chi.\mu^2} \sum_{i=1}^{n_{isotopes}} ab_i(Z + (A_i + (A_i - Z)f_{np})^2 \eta_{MB}(v_{min}, v_e) F(E_r, A_i)^2 \tag{2.10}$$

where m_U is amu in GeV, N_A is Avogadro's number, c is the speed of light, σ_p is the cross section for dark matter - proton interaction, m_χ is the dark matter mass and Z is the atomic number of the detector nucleus. The signal is a result of the nuclear recoil convoluted with the quenching factor, Q, due to the interaction of the detector nuclei with the dark matter particles. The quenching factor accounts for the fact that a nuclear recoil produces a different signal from an electronic recoil, which are used to calibrate the detector energy scale. For the case of a NaI detector, the quenching factors for Na and I are different (0.3 and .09 respectively). In the case of Xenon, there is only one quenching factor to account for (Q=.25). The energy in the detector can be written as

$$\frac{dR}{dE_{ee}}(E_{ee}, t) = \int_0^\infty dE_r \phi(E_{nr}, E_{ee}) \frac{dR}{dE_r}(E_r, t) \tag{2.11}$$

Because the scintillations are not detected with perfect resolution, the energy of the scintillation is detected up to the resolution of the detector. This enters the mesurement as the ϕ as defined below in relation to the $E_r = QE_{ee}$, where E_{ee} is the equivalent energy created by an electron recoil (electron equivalent). These units are picked because of the calibration methods for the detector.

$$\begin{aligned} \phi(E_{nr}, E_{ee}) &= \frac{1}{\sqrt{2}\pi\sigma^2(QE_r)} e^{-(E_{ee}-QE_r)^2/2\sigma^2(QE_r)} \\ \sigma(QE_r) &= \alpha\sqrt{Q}E_r + \beta QE_r \end{aligned} \tag{2.12}$$

where $E_e e$ is the measured electron equivalent energy for a given nuclear recoil of energy E_r. The $\frac{dR}{dE_{ee}}$ measured by DAMA can be decomposed to a DC signal, S_0, and an AC signal, S_m, the annual modulation. Here ω is the angular frequency for a one-year period and t_0 is a reference time chosen to coincide with the maxima of the signal, around June 1.

$$\frac{dR}{dE_{ee}}(E_{ee}, t) = S_0(E_{ee}) + S_m(E_{ee}) cos\omega(t - t_0) + ... \tag{2.13}$$

The sum of the modulations in certain bins (energy range 2-4 keV) is shown in Fig 2.1. The close fit to a cosinusoidal with a period of one year supports modeling the observed data in the form of a steady-state (S_0) component with an annually modulating (S_m) components. The energy spectrum of this modulation is further analysed as in Fig 2.2. Here, fits are done to the annual modulation signal assuming a single mass dark matter model. We construct a more general dynamical dark matter model that can not only reproduce these fits but expand the analysis with a more general approach.

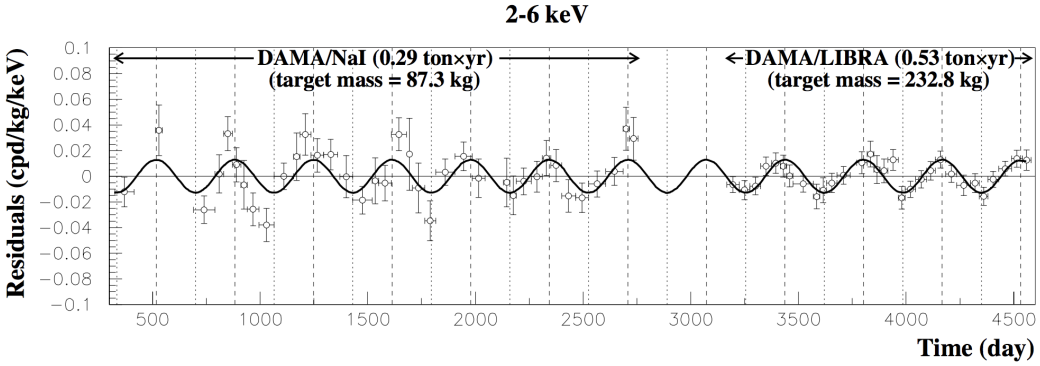

Figure 2.1: Annual Modulation signal: Sum of residuals of scintillation events in the 2-6 keVee energy bins after subtraction of time-averaged rate in each bin in each detector as a function of time. The zero on the horizontal axis is on January 1 1996 and this plot shows data for both DAMA/NaI and DAMA/LIBRA experiments. The overlayed curve shows a fit of the form $A\cos\omega(t - t_0)$ with ω equal to the angular frequency corresponding to a 1 year period and with the t_0 aligned such that the peak is on June 2. Figure from [18].

2.3 Compare Single mass vs. dynamical Dark Matter Models

For the case of dynamical dark matter model, instead of a single dark matter particle of mass χ, we have an ensemble of particles defined by m_0 and Δm. The densities and couplings of the higher mass particles are written in terms of the base particle and the parameters α, β and δ. Here, m_j is mass, Ω_j is cosmological density, f_{nj} is the ratio of the interaction cross sections with neutrons vs protons for the index j 'th particle in the ensemble. Using these, a quantity η can be defined that characterizes a particular ensemble. This parameter gives a measure of how 'dynamic' the ensemble will be as it gives the contribution to the relic density from the higher mass particles in the ensemble.

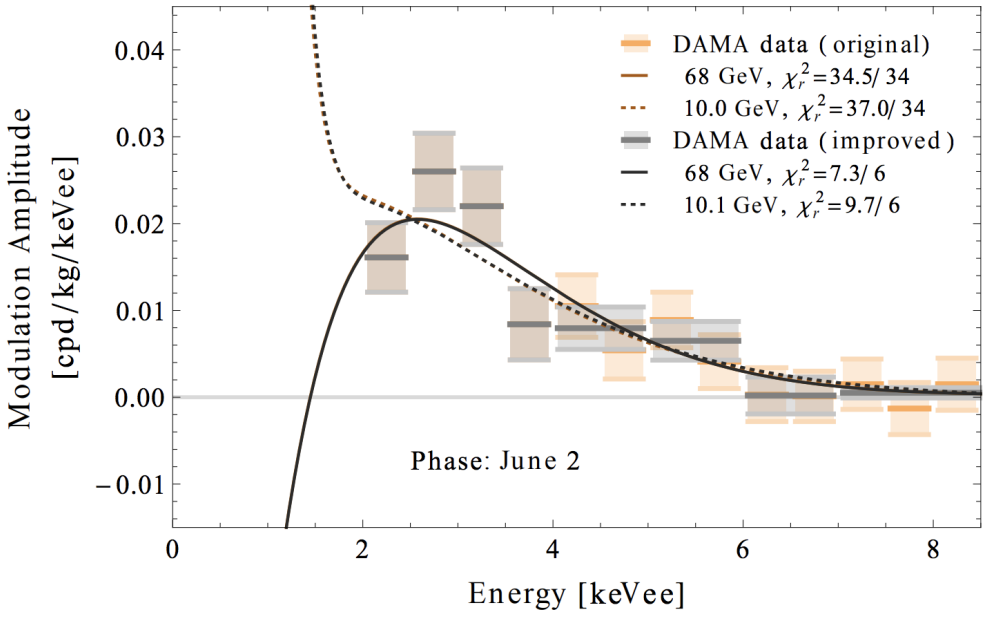

Figure 2.2: Annual Modulation signal: The average modulation amplitude by energy bin as measured by DAMA/LIBRA (orange boxes). Though not all shown here, measurements extend up to 20 keVee. To improve statistical sensitivity, some of the original bins have been combined (gray boxes): 6 original bins from 4-7 keVee have been combined into 3 bins with one final bin extending from 7-20 keVee (see the text for further discussion). The resulting bins are used for analyses in this paper. Also shown for both sets of binning are the modulation amplitude spectra for the WIMP mass and spin-independent (SI) cross-section that provides the global (solid line) and a local (dashed) chi-squared minima. Figure from [10].

$$
\begin{aligned}
m_j &= m_0 + j^\delta \Delta m \\
\Omega_j &= \Omega_0 (\frac{m_j}{m_0})^\alpha \\
f_{nj} &= f_{n0} (\frac{m_j}{m_0})^\beta \\
\Omega_{tot} &= \Omega_0 \sum_j \left(1 + j^\alpha \frac{\Delta m}{m_0}\right)^\alpha \\
\eta &= 1 - \left[\sum_j \left(1 + j^\alpha \frac{\Delta m}{m_0}\right)^\alpha\right]^{-1}
\end{aligned}
\tag{2.14}
$$

Now, the signal at a detector will be a weighted sum over all of these particles instead of a single χ at a mass of $m\chi$. Using this, we can modify equation (2.10) with the following.

$$\tilde{\eta}(m_0, \Delta m, \delta, \alpha) = \frac{1}{\sum_{j=0}^{j_{max}} (1 + j^{\delta} \frac{\Delta m}{m_0})^{\alpha}} \tag{2.15}$$

$$\frac{dR}{dE_r} = m_U N_A \frac{c^2 \rho_{DM} \sigma_p}{2 m_0 \mu^2} \tilde{\eta}(m_0, \Delta m, \delta, \alpha)$$
$$\cdot \sum_{i=1}^{n_{isotopes}} \sum_{j=0}^{j_{max}} a b_i (Z + (A_i + (A_i - Z) f_{np})^2 \eta_{MB}(v_{min}, v_e) F(E_r, A_i)^2 (1 + j^{\delta} \frac{\Delta m}{m0})^{\alpha+2\beta-1} \tag{2.16}$$

Now that we have an expression for the recoil spectrum, we can again use the energy resolution of the detector to give the expected signal. This is, once more, expanded as in eq 2.13 to get the single mass /dynamical model prediction of both the DC and AC (annual modulation) components of the dR/dE_{ee}. A consistency check for our DDM model can be performed as standard dark matter is the limiting case for DDM as $\Delta m = \infty$. We reproduce the previous results as in [10] for two best fit regions to the DAMA data: $m\chi = 10.1$ and 68.4 GeV, that fit to the DAMA data with χ^2 values of 9.7 and 7.3 (for 8 degrees of freedom) for cross sections of $1.1 \times 10^{-40}\text{cm}^2$ and $1.5 \times 10^{-41}\text{cm}^2$. Dynamical model predictions using $m_0 = 10.1$, $m_0 = 68.4$ and $\Delta m = \infty$, when plotted as crosses on the same plot, Fig 2.3, fall on the lines- demonstrating that for the limiting case, the dynamical dark matter model reduces to the single mass case.

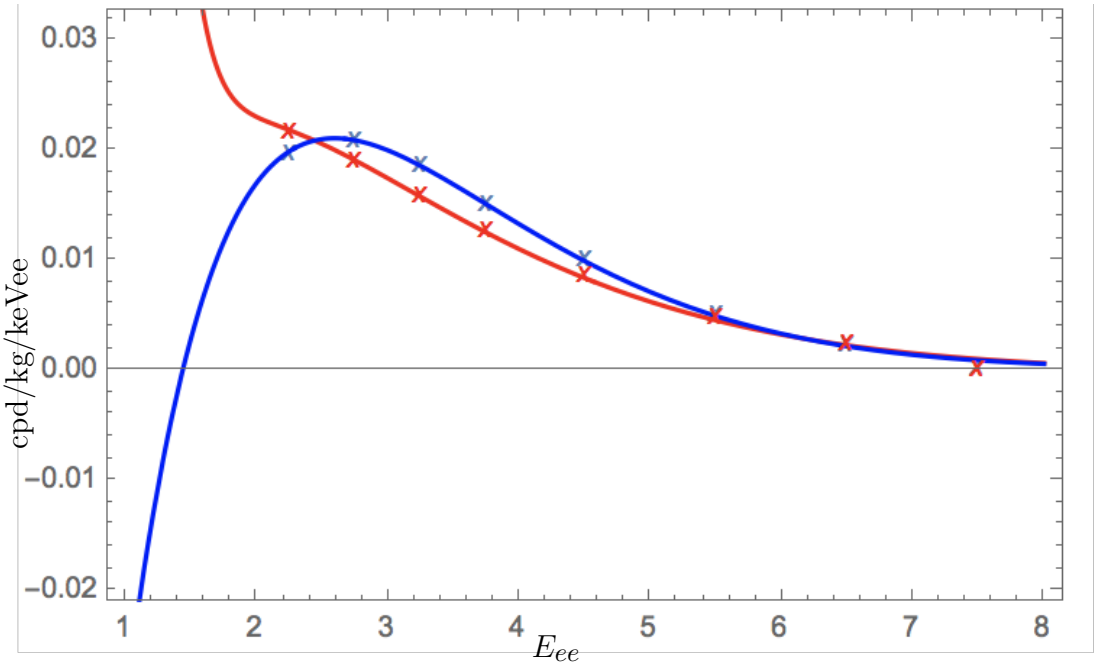

Figure 2.3: Annual Modulation signal: Non dynamical (lines) overlayed with dynamical signal with $\Delta m = \infty$ (crosses) red: $m\chi = 10.1$ GeV, blue: $m\chi = 68.4$ GeV. Notice that for the limiting case, the dynamical dark matter ensemble reduces to a single dark matter particle at $m\chi = m_0$ and the two results match.

2.4 Explore dynamical Dark Matter Parameter Space

With a preliminary check against a non dynamical model in the limiting case of $\Delta m \to \infty$ for the same elastic scattering cross section σ established, we now explore the space of m_0 and Δm that gives a χ^2 value less than 10 when fitted to the DAMA data (with rebinning as described in [10]: we are doing a goodness of fit using eight bins). We can see that a range of values produce a fit ($\chi^2 < 10$) for the dynamical dark matter ensemble.

We can see from the contour plots Figure 2.4 that for the allowed single mass case values of m_χ will lead to a possible signal for a range of Δm values in an ensemble model. For $m_0 \approx 10$ GeV, we see two islands, one at $\Delta m \approx 0$ and one for $\Delta m > 30$.

For all of these points, we use the same m_0, Δm and the interaction cross section

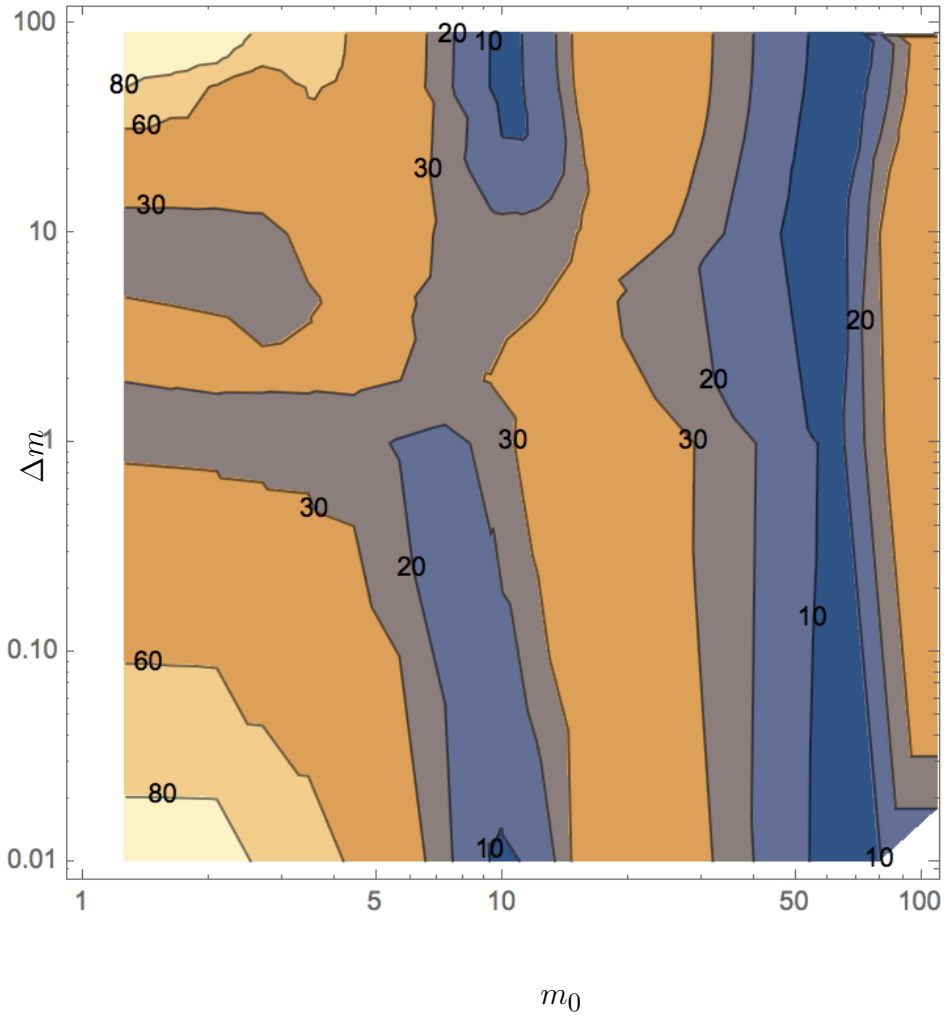

Figure 2.4: dynamical dark matter model fits: Contour plot of the χ^2 of the fit for the DAMA data rebinned to 8 bins . Notice that for $m_0 \approx (10,\ 68)$, a large set of Δm values (dark blue) leads to a good fit ($\chi^2 < 10$) for the data. For the smaller mass, the region appears as two disjoint islands, while for the higher mass case, a continuous region provides a good fit.

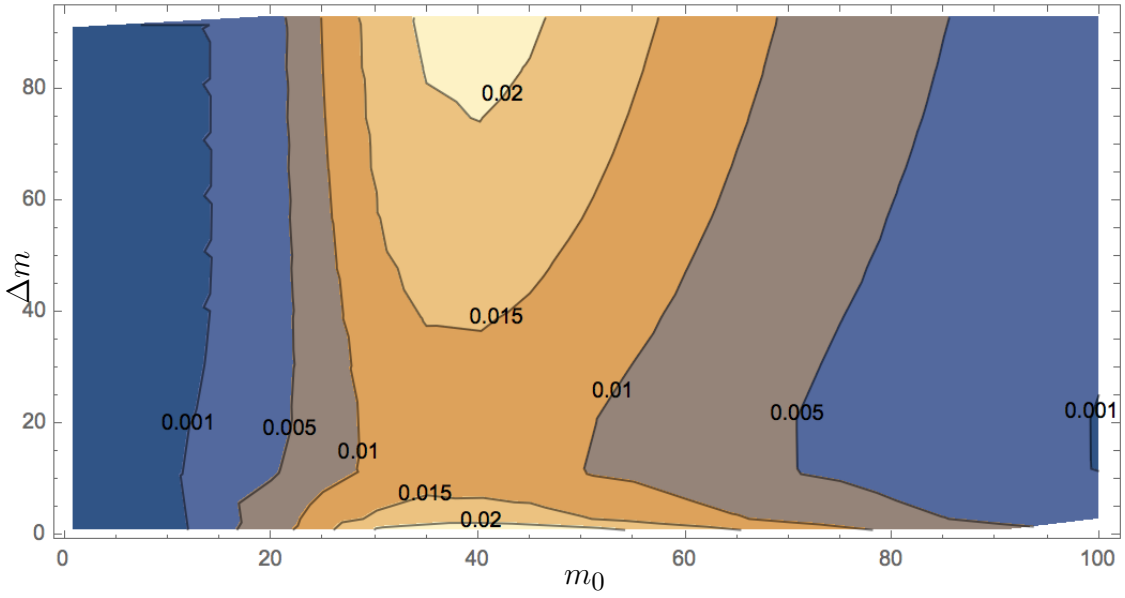

Figure 2.5: AC annual modulation signal projected for a Xenon detector for the values of m, Δm and σ considered for the NaI detector case. We notice that for points with $m = 30 - 70$, certain regions exceed the value of 0.01 cpd/kg/keVee.

and also calculate the DC and AC (annual modulation signal) projected for a Xenon detector. We find, in Fig 2.5, that for all points within the range m_0 : $(1, 100)$, Δm : $(.01, 100)$, the AC signal is well within limit (0.01 cpd/kg/keVee), but points with $m = 30 - 70$, certain regions exceed the value of 0.01 cpd/kg/keVee range- the resonance with Xenon is high in these intermediate mass regions. However, the DC signal is off limits (7×10^{-5} cpd/kg) for the entire range.

Having shown that a dynamical model explains current data just as well, with additional tunable parameters added, we look for features that can distinguish a dynamical model from a single-mass model. We compute the spectrum in Xenon detector in nine equal bins from 4-40 GeV. A dynamical signal is generated for a given m_0 and Δm- the Δm is chosen such that 95% of the relic density comes from the higher mass states. The error per bin is assumed to be predominantly statistical in

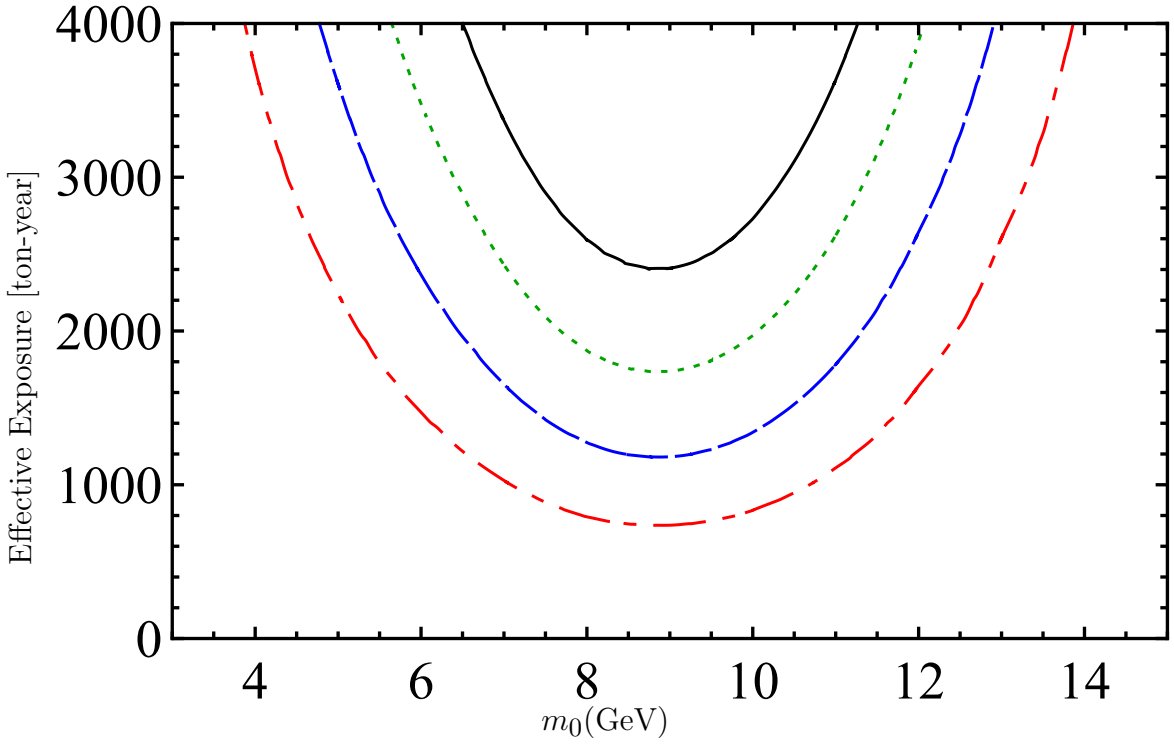

Figure 2.6: Limits for distinction between dynamical vs non dynamical models: The specific features in a dynamical spectrum can be distinguished from those of a non-dynamical model at various levels of exposure (red, blue, green, black: 2σ, 3σ, 4σ, 5σ). All these limits are beyond the current levels of exposures.

origin. To look for the best non-dynamical signal, a scan in mass and cross section is done to find the best fit using chi-squared test. Our statistical analysis depends only on the number of events observed at the xenon experiment, which is proportional to the exposure times the elastic scattering cross section. This means that we can present the results in terms of an effective exposure. This effective exposure is just the true exposure measured by an experiment, multiplied by the ratio of the true dark matter scattering cross-section to that of the current limits set by XENON1T. In Figure 2.6, we show the effective exposure that is required to distinguish our dynamical dark matter scenario from that of a traditional dark matter signal at the 2-5σ level using our goodness of fit test. We see that even if the dark matter cross section is right at the current limit, an exposure of more than 1000 ton-years is necessary for even

3σ evidence for distinguishing the model. This required exposure is well above any planned experiments and would be well into the neutrino floor meaning there would be an irreducible background due to neutrino interactions with the detector.

2.5 Conclusions and Future Work

We can see that regions of values of (m_0, Δm) for dynamical dark matter ensemble produce a good fit ($\chi^2 < 10$) for the DAMA data. In the limiting case of $\Delta m \to \infty$, these results are consistent with results of the non dynamical single mass dark matter case. For all of these points, we also calculate the DC and AC (annual modulation signal) projected for a Xenon detector find that for all points, the DC signal (7E-5 cpd/kg/keVee) is off limits. However, the AC signal is within range (0.01 cpd/kg/keVee) for two regions in the plot- at small masses (below 30) and then again at high masses (above 50). In the intermediate region, the signal due to Xenon resonance is high. In order to distinguish between a dynamical vs non-dynamical model using direct detection, we will need exposures on the order of 1000 ton-years, which is beyond the limits of currently planned experiments.

CHAPTER 3

DARK MATTER ANNIHILATION TO POSITRON AND ELECTRON

3.1 Introduction

From the measurements of the spectrum of cosmic ray positrons and electrons experiments including Fermi Gamma Ray Space Telescope [19] and PAMELA [20], we know not only the individual spectra, but also the positron fraction $[\Phi_{e^+}/(\Phi_{e^+ + e^-})]$. These measurements of two related quantities, say $(x + y)$ and $x/(x + y)$, can be used to constrain the size of possible features in these spectra, and hence the origin of these cosmic rays. One possible source of these cosmic rays is dark matter annihilation. Of particular interest, is the case in which two dark matter particles annihilate to produce a positron and an electron. This leads to a signature "bump" feature.

The results of the Alpha Magnetic Spectrometer (AMS-02) experiment [21], imminent at the time of this writing , are now out. AMS detects positrons and electrons in the cosmic ray spectrum between approximately 100 MeV and 1 TeV. With its much larger acceptance than PAMELA ($\sim$0.045 m^2sr vs. $\sim$0.002 m^2sr) [20] and its high level of proton rejection, AMS is expected to measure the cosmic ray positron flux as well as the positron fraction in far greater detail than was previously measured by PAMELA or Fermi.

In this article, we consider the case in which the dark matter particles annihilate directly to electron-positron pairs, giving rise to an edge-like feature in the cosmic ray positron spectrum at an energy equal to the mass of the annihilating WIMP [22, 23, 24]. Because of its increased precision, such features previously undetectable by PAMELA, might be detectable with AMS. We find that for dark

matter masses greater than ∼40 GeV, cross sections required to get a detectable spectral feature in the positron fraction are already ruled out due to the smoothness of the positron + electron spectrum as measured by Fermi.

We construct a model for the positron and electron flux to match with Fermi data. We add the primary and secondary electron and positron background with the flux from a nearby pulsar to get our background. For each dark matter model, we assume a NFW density profile and for a given annihilation cross section, we let the electrons and positrons to propagate through the galaxy using GALPROP [28]. GALPROP is a software tool that allows one to model various sources of cosmic particles as well as magnetic and electric fields in the galaxy, eventually allowing for the computation of cosmic particle spectra in the galaxy. The positron and electron spectrum detected at the position of the Sun is predicted using this code. For each mass, the dark matter annihilation leads to a feature in the spectrum that looks like an edge at the mass considered. We predict the spectrum assuming a particular binning for AMS. From the positron fraction spectrum, we calculate the cross section that is detectable with $\chi^2 = 4$, i.e. 95% confidence level, for the two adjacent bins. We then compare the positron + electron spectrum corresponding to the cross section with the Fermi data. We find that for masses from 25 to 800 GeV, cross sections that are detectable using the step in the positron fraction are ruled out by the lack of features in the positron + electron spectrum in the corresponding Fermi data.

3.2 Cosmic Ray Electrons and Positrons from Dark Matter Annihilation

Positrons and electrons produced by galactic sources, as well as due to dark matter annihilation, propagate through the galaxy under the influence of tangled magnetic

fields. Here they lose energy through inverse Compton and synchrotron interactions [25]. These effects can be modeled by the simple form of the diffusion-loss equation:

$$\frac{\partial}{\partial t}\frac{dn}{d\epsilon} = \ \bigtriangledown \cdot \left[K(\epsilon,\vec{x})\vec{\bigtriangledown}\frac{\partial n}{\partial \epsilon}\right] + \frac{\partial}{\partial \epsilon}\left[b(\epsilon,\vec{x})\frac{\partial n}{\partial \epsilon}\right] + Q(\epsilon,\vec{x}) \tag{3.1}$$

where n is the number density, $\epsilon = E/(1\ \mathrm{GeV})$ parametrizes the energy of cosmic ray particles, K is the diffusion constant (denoted D_{xx} in GALPROP), b is the energy loss rate, and Q the source term, i.e. the source of particles in units of $\mathrm{cm}^3\mathrm{s}^{-1}$ [25]. For the general case of particles produced by self-annihilations:

$$Q(\vec{x},\epsilon) = \frac{1}{2}\frac{\rho^2(\vec{x})}{m^2}\sigma v\frac{dN}{d\epsilon} \tag{3.2}$$

where $dN/d\epsilon$ is the spectrum of the resultant particles per annihilation as a function of energy. In the case of annihilation to electron and positron final states, $dN/d\epsilon = 2\delta(m)$, where m is the mass of the dark matter particles. In order to find a steady state solution for the spectrum $dn/d\epsilon$, the left hand side is set to zero and the solution is carried out as detailed in Ref [25].

We are interested in looking at the positron and electron spectrum and searching for dark matter signal. We assume an NFW dark matter halo profile [26] with the local dark matter density, $\rho_0 = 0.43\ \mathrm{GeVcm}^{-3}$. In particular, we consider a model where two dark matter particles of a particular mass annihilate into a positron and an electron, which then propagate through the galaxy and are detected on/near Earth.

In this case, Q, the source term depends on the dark matter annihilation cross section as well as the inhomogeneity of the distribution (leads to a boost factor- to account for the difference in collision rates due to the variation in densities- which we take to be 1). The energy loss rate, $b = 10^{-16}(E/GeV)^2$, is the result of inverse Compton scattering on starlight and the cosmic microwave background, and

synchrotron radiation due to the galactic magnetic field. Following Ref. [27], we expect a spectrum with an edge feature at the mass of the dark matter which is:

$$\frac{dn}{d\epsilon} = \frac{Q(m_{dm}, x_0)}{b}\theta(m_{dm} - \epsilon) \tag{3.3}$$

Following Ref. [25] we evaluate the size of this feature using $Q = n_0^2 < \sigma v > m_{dm}^{-2}$ for a model dark matter that annihilates to electrons and positrons, where n_0 is the number density. We will use this for a simple check to verify the number obtained from GALPROP. Following Ref. [25] again, we calculate that the detected flux at the edge of a particular dark matter mass to be:

$$\frac{d\Phi}{d\epsilon} = \frac{c}{4\pi}\frac{dn}{d\epsilon} \tag{3.4}$$

For the case of $m_{dm} = 130$ GeV, with a cross section of $3\text{x}10^{-26}$ cm^3s^{-1}, we calculated this edge size to be $E^3 d\Phi/dE = 4.9\,\text{GeV}^2\text{m}^{-2}\text{sr}^{-1}\text{s}^{-1}$, which matches closely with the value of $4.8\,\text{GeV}^2\text{m}^{-2}\text{sr}^{-1}\text{s}^{-1}$ we obtained through our GALPROP simulation.

To determine the cosmic ray spectrum as observed at the Solar System, we solve the standard propagation equation (using the publicly available code GALPROP [28]):

$$\begin{aligned}\frac{\partial\psi}{\partial t} = \; & Q(\mathbf{r}, p) + \bigtriangledown \cdot (D_{xx} \bigtriangledown \psi - \mathbf{V}\psi) + \frac{\partial}{\partial p}p^2 D_{pp}\frac{\partial}{\partial p}\frac{1}{p^2}\psi \\ & -\frac{\partial}{\partial p}\left[\dot{p}\psi - \frac{p}{3}\left(\bigtriangledown \cdot \mathbf{V}\right)\psi\right] - \frac{1}{\tau_f} - \frac{1}{\tau_r}\psi \;,\end{aligned}$$

where $\psi(\mathbf{r}, p, t)$ is the number density of a given cosmic ray species per unit momentum, p, and the source term $Q(\mathbf{r}, p)$ includes the products of the decay and spallation of nuclei, as well as any primary contributions from supernova remnants, pulsars, dark matter annihilations, etc., $\mathbf{V}$ is the convection velocity, D_{xx} is the

spatial diffusion coefficient, which is parametrized by $D_{xx} = \beta D_{0xx}(\rho/4GV)^{\delta}$, where β and ρ are the particle's velocity and rigidity, respectively, while the terms with τ account for decay of particles. Also included in this equation are the effects of diffusive reacceleration and radioactive decay [28], however we neglect the effects of convection. The contribution to the source term, $Q(\mathbf{r}, p)$, from dark matter is simply determined by the flux of annihilation products injected into the halo. In our calculations, we adopt $D_{0xx} = 4.02 \times 10^{28}$ cm^2/s and apply free-escape boundary conditions at 4 kpc above and below the Galactic Plane. These choices lead to boron-to-carbon and antiproton-to-proton ratios that are consistent with observations [30, 29].

3.3 Astrophysical Sources of Cosmic Ray Electrons and Positrons

We model the background positron and electron flux to match the measurements made by Fermi. Primary sources of electrons include supernova remnants and pulsars. Secondary electrons and positrons are those created by collisions of cosmic rays which occur during propagation through the galaxy. We account for the overall flux as a sum of these primary and secondary electrons and positrons combined with the flux from one nearby supernova remnant Monogem and the associated pulsar B0656+14. This pulsar is located 290 parsecs from the Solar System and is 110,000 years old [31]. We assume this pulsar to have injected a spectrum of positrons and electrons of the form, $Q \propto E_e^{-1.7}$. We follow Ref. [32] in determining the flux of positrons and electrons at the Solar System from this pulsar and add this to the contribution predicted from primary and secondary production, as obtained using GALPROP.

The cosmic ray spectrum as observed by detectors close to the Earth is further affected by solar winds and heliospheric magnetic field [33]. This effect modeled by

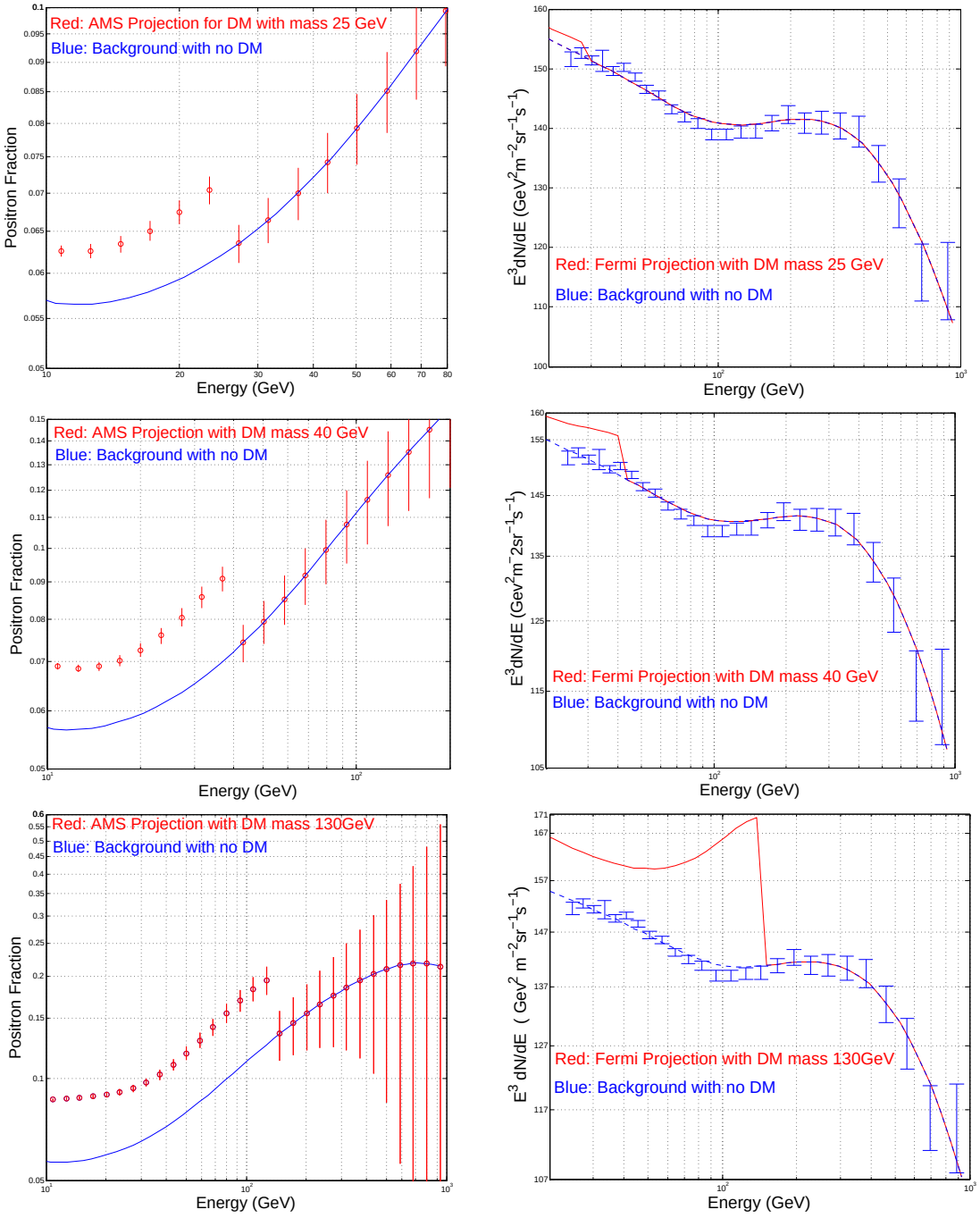

Figure 3.1: Left: Projection for AMS's measurement of the positron fraction for the case of dark matter with masses 25 GeV ($\sigma v = 1.5 \times 10^{-27}$ cm^3/s), 40 GeV ($\sigma v = 1.5 \times 10^{-26}$ cm^3/s) and 130 GeV ($\sigma v = 9 \times 10^{-26}$ cm^3/s) annihilating to e^+e^-. These cross sections were picked such that $\chi^2 = 4$ for the midpoint of the two bins adjacent to the step, corresponding to detection of a sudden spectral feature at the 95% confidence level. Right: Total electron + positron flux, compared with Fermi data (blue error bars) for the same dark matter scenarios shown in the left panels. Although we cannot rule out the possibility that AMS could detect a sudden spectral feature at energies below $\sim$ 40 GeV, it is obvious that any higher energy feature potentially observable by AMS is already ruled out by Fermi.

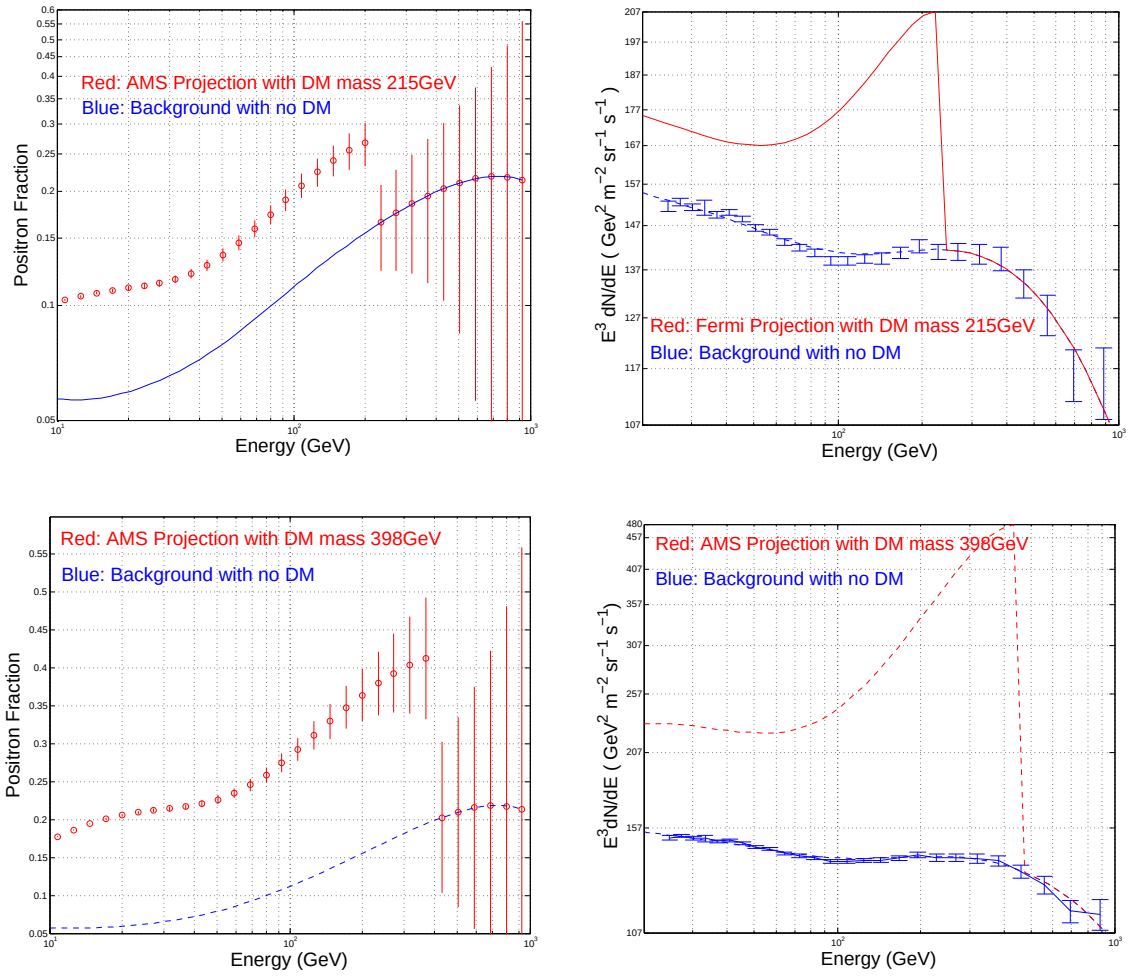

Figure 3.2: Left: Projections for AMS measurement of positron fraction for the cases of dark matter with masses 215 ($\sigma v = 3.3{\times}10^{-25}$ cm^3/s) and 398 GeV($\sigma v = 3{\times}10^{-24}$ cm^3/s) annihilating to e^+, e^-. These cross sections were picked such that $\chi^2 = 4$ for the midpoint of the two bins adjacent to the step, corresponding to detection of a sudden spectral feature at the 95% confidence level. Right: Total electron + positron flux, compared with Fermi data. It is clear that these are ruled out by Fermi data. Considering the trend, we conclude that the requisite cross section for higher masses is still greater and therefore we do not show further plots for higher masses.

an effective potential, $\Phi = 0.4$ GeV, is especially important for energies smaller than roughly 20 GeV. The interstellar cosmic ray flux J_{IS} is related to the observed flux, J, as shown below:

$$J(p) = \frac{p(p+2m_p)}{(p+\Phi)(p+\Phi+2m_p)} J_{IS}, \tag{3.5}$$

with p, again, being the momentum. To project the error bars for AMS, we follow Ref. [34]. We convolve the positron fraction spectrum with an energy resolution of $\Delta E/E = \sqrt{(0.106/\sqrt{E(\mathrm{GeV})})^2 + (0.0125)^2}$ (corresponding to about 3.5% at 10 GeV), an ability to reject protons from positrons and protons from electrons at the level of 3×10^5 [35], positrons from electrons at 1×10^4 and an acceptance of 0.045 m^2 sr. We are assuming 15 bins per decade. While we have calculated our error bars for 3 years of data taking, the systematic rather than statistical errors dominate the results.

3.4 Incompatibility with Fermi Constraints

For a series of dark matter masses between 25 and 1000 GeV (which is the range covered by existing Fermi data), we determine the cross section required to produce a step in the positron fraction discernible by AMS. For a spectral feature that can be detected at the 95% confidence level, we require $\chi^2 \geq 4$ for the two bins adjacent to the step.

When we plot the positron + electron spectrum alongside our fit to Fermi data, we find that in most cases the corresponding feature would be incompatible with the existing Fermi data. This is shown in Figures 3.1 and 3.2. We can conclude that for all masses above $\sim$40 GeV, the existence of dark matter particles that annihilate into positrons and electrons to produce a feature detectable by AMS is already ruled out

by Fermi. One special point is the the case of $m_{dm} = 130$ GeV. It has been speculated that a spectral gamma ray feature observed by Fermi around 130 GeV may be related to signals from dark matter annihilations to $\gamma\gamma$, γZ or γh [36, 37]. As no continuum gamma ray signal is observed, however, there is a motivation to consider 130 GeV dark matter particles that annihilate to final states such as electrons and positrons [38] . We show in row 3 of Figure 3.1 the predictions for this dark matter mass. We conclude that AMS is unlikely to observe a spectral feature associated with dark matter of this mass assuming dark matter particles annihilate strongly into positrons and electrons.

3.5 Conclusion

Looking for dark matter is one of the missions of the AMS detector. We consider dark matter models where two dark matter particles annihilate to produce an electron-positron pair giving rise to a signature bump at the mass of the annihilating particles. From our calculations we see that for masses greater than ∼40 GeV, the cross sections corresponding to a detectable feature in the positron fraction spectrum of AMS are already ruled out by existing Fermi measurements of the positron+ electron spectrum.

Now, that the AMS data has been out, we observed that there were no strong features in the region ruled out by our study, hence these results were validated.

REFERENCES

[1] J. H. Jeans, Mon.Not.Roy.Astron.Soc. 82, 122 132 (1922).

[2] F. Zwicky, Helv.Phys.Acta 6, 110 127 (1933).

[3] J. Einasto, arXiv:0901.0632.

[4] D. Clowe, M. Bradac, A. H. Gonzalez, M. Markevitch, S. W. Randall, et al., A direct empirical proof of the existence of dark matter, Astrophys.J. 648 (2006) L109L113, arXiv:astro-ph/0608407 [astro-ph].

[5] D. Hooper, Particle Dark Matter 0901.4090 [hep-ph] —

[6] A. Borriello and P. Salucci, The Dark matter distribution in disk galaxies, Mon.Not.Roy.Astron.Soc. 323 (2001) 285, arXiv:astro-ph/0001082 [astro-ph].

[7] H. Hoekstra, H. Yee, and M. Gladders, Current status of weak gravitational lensing, New Astron.Rev. 46 (2002) 767781, arXiv:astro-ph/0205205 [astro-ph].

[8] L. A. Moustakas, K. Abazajian, A. Benson, A. S. Bolton, J. S. Bullock, et al., Strong gravitational lensing probes of the particle nature of dark matter, arXiv:0902.3219 [astro-ph.CO].

[9] N. Jarosik, C. Bennett, J. Dunkley, B. Gold, M. Greason, et al., Astrophys.J.Suppl. 192, 14 (2011), [arXiv:1001.4744].

[10] Kelso C. et al., Lowering the Threshold in the DAMA Dark Matter Search , *MCTP-13-14, NSF-KITP-13-104, CETUP2013-004*, arXiv:1306.1858[astro-ph.CO].

[11] Keith R. Dienes, Jason Kumar, Brooks Thomas, [arXiv:1208.0336v2 [hep-ph]] (09-27-2012)

[12] K. Abe et. al, XMASS Collaboration [arXiv:1801.10096v1[astro-ph.CO]](30 Jan 2018)

[13] R. Bernabei, P. Belli, F. Cappella, R. Cerulli, F. Montecchia, F. Nozzoli, A. Incicchitti and D. Prosperi *et al.*, Riv. Nuovo Cim. **26N1**, 1 (2003) [astro-ph/0307403].

[14] R. Bernabei *et al.* [DAMA Collaboration], Nucl. Instrum. Meth. A **592**, 297 (2008) [arXiv:0804.2738 [astro-ph]].

[15] R. Bernabei *et al.* [DAMA and LIBRA Collaborations], Eur. Phys. J. C **67**, 39 (2010) [arXiv:1002.1028 [astro-ph.GA]].

[16] A. Bottino, F. Donato, N. Fornengo and S. Scopel, Phys. Rev. D **68**, 043506 (2003) [hep-ph/0304080].

[17] R. H. Helm, Phys.Rev. 104 (1956) 1466?1475.

[18] C. Kelso, PhD Dissertation. http://lss.fnal.gov/archive/thesis/2000/fermilab-thesis-2012-32.pdf

[19] Fermi LAT Collaboration, M. Ackermann *et al.*, Phys.Rev.Lett. **108**, 011103 (2012), 1109.0521.

[20] PAMELA Collaboration, O. Adriani *et al.*, Nature **458**, 607 (2009), 0810.4995.

[21] AMS Collaboration (J. Alcaraz et al.). Physics Reports 366: 331405, 2002. 74pp.

[22] E. A. Baltz and D. Hooper, JCAP **0507**, 001 (2005), hep-ph/0411053.

[23] G. Bertone, D. Hooper and J. Silk Phys.Rept.405:279-390,2005, arXiv:hep-ph/0404175v2

[24] D. Hooper and J. Silk Phys.Rev. D71 (2005) 083503, arXiv:hep-ph/0409104

[25] E. A. Baltz and J. Edjso Phys.Rev.D59:023511,1998

[26] J F. Navarro, C. S. Frenk and S. D. M. White Astrophys.J.462:563-575,1996

[27] E. A. Baltz and D. Hooper JCAP 0507:001,2005

[28] A. Strong and I. Moskalenko, Astrophys.J. **509**, 212 (1998), astro-ph/9807150.

[29] M. Simet and D. Hooper, JCAP 0908:003,2009

[30] D. Hooper and K M Zurek, arXiv:0909.4163 [hep-ph]

[31] V. Barger et al. Phys.Lett.B678:283-292,2009. 0810.4994. arXiv:0904.2001 [hep-ph]

[32] D. Hooper, P. Blasi, and P. D. Serpico, JCAP **0901**, 025 (2009), 0810.1527.

[33] L. J. Gleeson and W. I. Axford, Astrophys. J. 154 1011 (1968)

[34] M. Pato, M. Lattanzi, and G. Bertone, JCAP **1012**, 020 (2010), 1010.5236.

[35] J. Casaus, J.Phys.Conf.Ser. **171**, 012045 (2009).

[36] C. Weniger arXiv:1204.2797 [hep-ph]

[37] D. P. Fiinkbeiner, M. Su, C Weniger arXiv:1209.4562 [astro-ph.HE]

[38] M. R. Buckley and D. Hooper arXiv:1205.6811 [hep-ph]

[39] O. Adriani *et al.*, Phys.Rev.Lett. **102**, 051101 (2009),

[40] S. Profumo, Central Eur.J.Phys. **10**, 1 (2011), 0812.4457.

[41] M. Pato, D. Hooper, and M. Simet, JCAP **1006**, 022 (2010), 1002.3341.

[42] D. Hooper and T. Linden, Phys.Rev. **D84**, 123005 (2011), 1110.0006.

[43] D. Hooper and W. Xue, arXiv:1210.1220 [astro-ph.HE]

[44] D. Grasso et al. Astropart.Phys.32:140-151,2009

[45] E A Baltz, J Edsjo, Phys.Rev.D59:023511,1998

[46] I. V. Moskalenko, A. W. Strong, J. F. Ormes, and M. S. Potgieter, Astrophys.J. **565**, 280 (2002), astro-ph/0106567.